CrystEngComm

Accepted Manuscript

ROYAL SOCIETY OF CHEMISTRY

www.rsc.org/crystengcomm

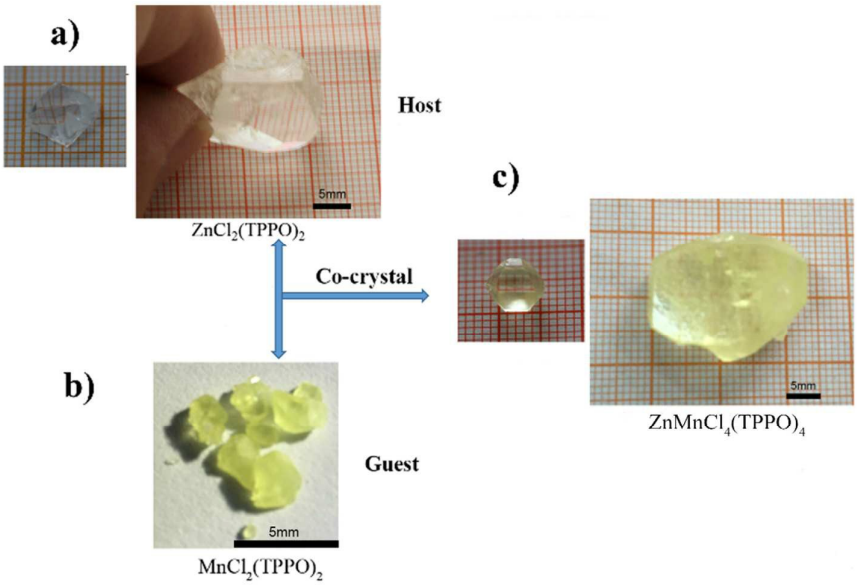

In this study, hybrid semi-organic crystal of $ZnMnCl_4(TPPO)_4$ for second-order nonlinear, magnetic, luminous applications have been designed, synthesized and grown from a guest-host combination of $MnCl_2(TPPO)_2$ and $ZnCl_2(TPPO)_2$ and the formation is bidirectional.

Journal Name

RSCPublishing

ARTICLE

Cite this: DOI: 10.1039/x0xx00000x

New Potential Nonlinear Optical Hybrid Semi-Organic Crystal of $ZnMnCl_4(TPPO)_4$ with attractive physical properties †

Received 00th January 2012,
Accepted 00th January 2012

DOI: 10.1039/x0xx00000x

www.rsc.org/

Xiaolong Liu, Guangqiang Wang,Yangyang Dang, Shaojun Zhang, Hanlin Tian, Yan Ren* and Xutang Tao*

This paper describes the crystal growth, structure and properties of a new semi-organic hybrid crystal with accurate molecular formula of $ZnMnCl_4(TPPO)_4$ by a guest-host combination of $ZnCl_2(TPPO)_2$ and $MnCl_2(TPPO)_2$ for the first time and the formation is bidirectional. It crystallizes in the acentric space group *F*dd2. The 3D framework of the crystal structure is formed by triphenylphosphine oxide (TPPO), connected with a mixture of Zinc (II) chloride and Manganese (II) chloride. A mixed occupancy of zinc and manganese atoms was designed to form a noncentrosymmetric coordination compound, which exhibits the relatively strong second-order nonlinear properties. The powder of these crystal shows phase-matchable SHG effect that is twice that of KH_2PO_4 (KDP). The crystal has a broad optical transmission range, relatively good stability and a wide band gap. It is also magnetic and luminescent. The properties of this new make it a potential candidate for improved or even novel devices.

1. Introduction

Nonlinear optical (NLO) materials are of great interest due to their potential application as laser frequency converters, optical parameter oscillators (OPOs), and for signal communication and detection.[1-4] Several other NLO crystals, such as KH_2PO_4 (KDP),[5] $KTiOPO_4$ (KTP),[6] LiB_3O_5 (LBO),[7] β-BaB_2O_4 (BBO),[8] $LiNbO_3$,[9] $KBe_2BO_3F_2$ (KBBF)[10] and N,Ndimethylamino-N'-methylstilbazolium-p-toluenesulfonate (DAST),[11,18] etc. have found wide application. Inorganic crystal materials, such as $BaTeMo_2O_9$ (BTM),[12] $Cs_2TeMo_3O_{12}$ (CTM),[13] $Na_2TeW_2O_9$ (NTW)[14] and $Cs_2TeW_3O_{12}$ (CTW)[15] have been well developed previously by our research group for NLO. Compared with inorganic crystal materials, organic NLO crystal materials exhibit large second-harmonic generation (SHG) and electro-optic coefficients, low dielectric dispersion, ultrafast response times and highly tailorable structures together with a high laser damage thereshold.[16-17] However, since nearly 75% of organic crystals crystallize in centrosymmetric space groups, which exhibit no SHG[18], the search for new NLO organic crystals with noncentrosymmetric structures is of great importance.

Strategies to induce crystallization in a noncentrosymmetric arrangement mainly include the following: attachment of a chiral handle, crystallizing the molecules in a chiral inclusion mixture,[19-20] utilization of polar solvents to obtain an acentric structure [21] and rendering materials useful as guest-host mixed crystals.[22] In the past, our research group has synthesized a series of crystal materials for NLO properties. For example, MHBA,[23] LATF,[24] G2HP[25] and TDCB.[26]

Previously, semi-organic crystal with one metal cation, such as $Cu(TPPO)_4X_2 \cdot 2H_2O$ (X= Cl, Br)[27] and $CdI_2(TPPO)_2$[28], etc. have been made for magnetic and nonlinear adhibition. Scale-up crystal of $CdI_2(TPPO)_2$ with high quality have been grown with temperature lowering method. However, limited by the aggregation pattern of the molecular, small SHG response has been acquired. For $Cu(TPPO)_4X_2 \cdot 2H_2O$ (X= Cl, Br) complex, blue and green crystals have been prepared and ferromagnetic interaction was revealed. However, the implement of large SHG response or even multitudinous physicochemical properties are untoward for semi-organic crystal with one metal cation.

Herein, hybrid semi-organic crystals of $ZnMnCl_4(TPPO)_4$ have been designed, synthesized and grown for second-order nonlinear, magnetic and luminous applications for the first time. The growth habit of $ZnCl_2(TPPO)_2$ (host) is good but not of $MnCl_2(TPPO)_2$ (guest), so a guest-host combination was designed. Moreover, the advantages of both crystals only were

integrated for the presentation of unique physicochemical properties. High quality hybrid semi-organic crystals of $ZnMnCl_4(TPPO)_4$ have been obtained using the temperature lowering method. Properties of the crystal including the structure, transmittance spectrum, thermal stability, band gap, magnetic, luminescence, and nonlinear optical properties are reported in detail. Also structure and part of the properties of $ZnCl_2(TPPO)_2$ were exhibited to prove the formation of the hybrid semi-organic crystal.

2. Experimental section

2.1 Reagents

Triphenylphosphine oxide (98%), Zinc (II) chloride (AR), Manganese (II) chloride tetrahydrate (AR) and ethanol (HPLC) were purchased from J&K Scientific Ltd. All starting materials were used without further purification.

2.2.1 Synthesis and crystal growth of $ZnCl_2(TPPO)_2$.

Zinc (II) chloride (0.05 mol, 6.815 g) and triphenylphosphine oxide (0.10 mol, 27.829 g) were added to ethanol in a round-bottom flask. The solution was heated to 65℃ and stirred for 4 hours, until the turbid solution became clear and colourless. The solution was then filtered quickly and put into a wide-mouth bottle. The solution was cooled slowly to the room temperature at the speed of 0.5 °C/day. Bulk optical colourless crystals appeared during this process. (See Fig.2)

2.2.2 Synthesis and crystal growth of $Zn_{0.5}Mn_{0.5}Cl_2(TPPO)_2$.

Zinc (II) chloride (0.02 mol, 2.727 g), Manganese (II) chloride tetra hydrate (0.02 mol, 3.249 g) and triphenylphosphine oxide (0.08 mol, 22.262 g) were put into a round-bottom flask together with ethanol. The mixture was stirred at 65°C for 4 h until the muddy brown mixture became a clear golden yellow solution. The solution was then filtered quickly and put into a wide-mouth bottle. The solution was cooled slowly to the room temperature with at the speed of 0.25°C/day. Bulk high quality light yellow crystal appeared during this process. (See Fig.2)

2.3 Powder X-ray diffraction

The X-Ray powder diffraction (XRD) was performed using a Bruker-AXS D8 ADVANCE X-Ray diffractometer, with Cu-Kα radiation (λ = 1.54186 Å) in the range of 10°-90° using a step size of 0.1° and reasonable step time settings. Powder XRD patterns for $ZnMnCl_4(TPPO)_4$ were obtained from polycrystalline material after recrystallization. The XRD patterns showed good agreement with calculated XRD patterns based on the single crystal structure analysis.

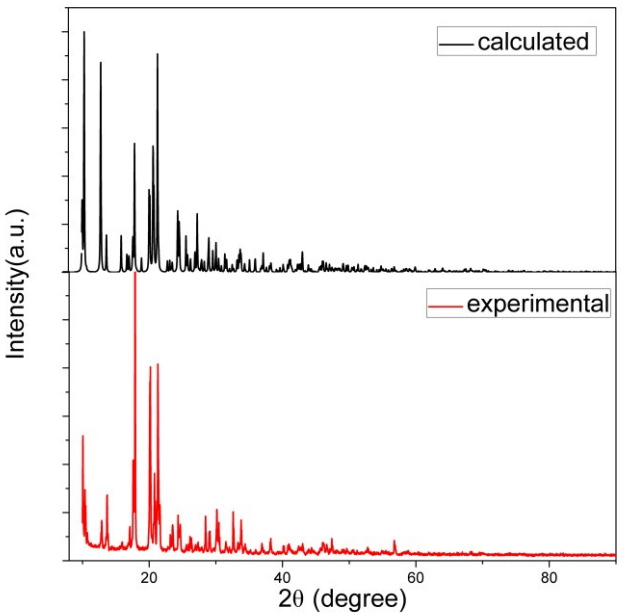

Fig. 1 The experimental and calculated XRD patterns of $MnZnCl_4(TPPO)_4$.

2.4 X-ray crystal structure determination.

Table 1 Crystal data and structure refinements for $ZnMnCl_4(TPPO)_4$

Formula	C_{72} H_{60} O_4 P_4 Mn Zn Cl_4
Formula weight/g mol^{-1}	1375.19
T/K	296(2) K
Wavelength/Å	0.71073
Crystal size/mm^3	0.15×0.13×0.12
Crystal colour	Light yellow
Space group	*F*dd2(No.43)
a/Å	20.7414(14)
b/Å	32.981(2)
c/Å	9.7539(7)
α/deg	90
β/deg	90
γ/deg	90
Volume/$Å^3$	6672.4(8)
Z	4
Calculated density /g·cm^{-3}	1.369
μ/mm^{-1}	0.853
Limiting indices	-20<=h<=26, -39<=k<=42, -12<=l<=12
Absolute structure Flack	-0.063(11)
F (000)	2828
Reflections collected	9887
θ range (°)	2.32 ~27.53
Reflections collected / unique	9887/ 3570 [R(int) = 0.0164]
Gof	1.074
Data / restraints / parameters	3570 / 1 / 196
R_1, wR_2 [I >2σ(I)]	R_1 = 0.0243, wR_2 = 0.0665
R_1, wR_2 (all data)	R_1 = 0.0253, wR_2 = 0.0671
Extinction coefficient	0.00138(8)
Min/Max Δρ/e$Å^{-3}$	-0.261/ 0.444

[a]$w = 1/[s^2(Fo^2)+(0.0325P)^2+3.0996P]$, where $P = (Fo^2+2Fc^2)/3$.

High quality single crystals of $ZnCl_2(TPPO)_2$ and $ZnMnCl_4(TPPO)_4$ were selected for crystal structure analysis. Data sets were collected using a Bruker SMART APEX-II diffractometer equipped with a CCD detector (graphite-

monochromatic Mo-Kα radiation, λ= 0.71073 Å) at 293(2) K. APEX2 software[29] was used for data integration and cell refinement. The structure was determined and verified using SHELXTL 97 software.[30]

Table 2. Macro-statistics average bond lengths [Å] and angles [deg] for $ZnMnCl_4(TPPO)_4$.

Zn (1)-O (2) or (Mn)(1)-O	1.9796(12)
Zn (1)-Cl (1) or Mn) (1)-Cl	2.2091(5)
P (2)-O (2)	1.5021(11)
P (2)-C (1)	1.7972(17)
C (1)-C (4)	1.391(3)
O#1-Zn (1)-O or O#1-Mn (1)-O	96.71(8)
O#1-Zn (1)-Cl or O#1-Mn (1)-Cl	112.18(4)
O-Zn(1)-Cl or O- Mn(1)-Cl	108.94(4)
Cl#1-Zn(1)-Cl or Cl#1-Mn(1)-C	116.21(3)
C(1)-P(2)-C (7)	109.92(8)
C(4)-C(1)-C (9)	119.46(17)
O(2)-P(2)-C (1)	111.48(8)
P(2)-O(2)-Zn(1) or P(2)-O(2)-Mn (1)	153.12(9)

Symmetry transformations used to generate equivalent atoms:

#1 -x+1/2,-y+1/2, z

The elemental ratio of Zn to Mn in the hybrid semi-organic crystal was determined with X-ray fluorescence (XRF) using ZSX Primus II equipment with resolution 139±5eV. (See Table S2 in ESI.†) Further details of the crystal structures of $ZnCl_2(TPPO)_2$ and $ZnMnCl_4(TPPO)_4$ can be obtained from the Cambridge Structural Database (CSD) of WebCSD with registry CCDC numbers 1442330 and 1057044, respectively.

2.5 Optical characterization.

The transmittance of $ZnMnCl_4(TPPO)_4$ was measured on a Hitachi U-3500 spectrometer, which has an operating range of 200–3200 nm at room temperature, using plates that were 4×4×1 mm. The fluorescence spectrum was obtained using a Hitachi F-4500 fluorescence spectrophotometer. The UV–Vis diffuse reflectance spectrum was recorded on a Shimadzu UV–Vis 2550 spectrophotometer equipped with an integrating sphere over the spectral range 200–900 nm. A $BaSO_4$ plate was used as a standard (100% reflectance), on which the finely ground samples from the crystals were coated. The absorption spectra were calculated from the reflectance spectrum using the Kubelka–Munk function:

$$\alpha/S= (1-R)^2/(2R).^{31}$$

Where α is the absorption coefficient, S is the scattering coefficient, and R is the reflectance.

2.6 Thermo gravimetric analysis and Differential Thermal Analysis.

Thermo-gravimetric analysis (TGA) and differential thermal analysis (DTA) were carried out on a TGA/DTA 1/1600HT analyzer (METTLER TOLEDO Instruments). A ground crystal sample of $ZnMnCl_4(TPPO)_4$ weighing 2.932mg was placed in a Pt crucible and heated from 30 °C to 600 °C at a heating rate of 10 K/min^{-1} under flowing nitrogen.

2.7 Hardness test.

The hardnesses of $ZnMnCl_4(TPPO)_4$ and $ZnCl_2(TPPO)_2$ were estimated using an HXD-1000C micro-hardness tester on (010)-faced plates with dimensions of 4 × 4 × 1 mm. The indentation load was 10g and the selected time was 2s. The micro hardness (Hv) and Mohs hardness (HM) values were calculated using the following relations.The tests were performed eight times, and the Hv_{min} and Hv_{max} were removed before averaging.

$$Hv=1.8544 \times (p/ d^2)\ kg\times mm^{-2}$$

$$Hm= 0.675 \times (Hv)^{1/3}$$

2.8 Magnetic property measurements.

The temperature dependence of the magnetic susceptibility of $ZnMnCl_4(TPPO)_4$ single crystal was measured on a Quantum Design SQUID MPMS XL-7 instrument in the temperature range 5–300 K with a field of 1000 Oe. The temperature dependence of χM and χM^{-1} are displayed in Fig. 8.

2.9 Second-harmonic generation measurements.

The SHG of the samples were investigated using a Kurtz–Perry powder technique.[32] Polycrystalline samples of $ZnMnCl_4(TPPO)_4$ and KDP were ground and sieved to obtain distinct grain sizes. The sieved KDP powders of the same size ranges were used as the reference. The samples were pressed between glass microscope cover slides and secured with tape in 0.45 mm thick aluminum holders, which contained a 3 mm diameter hole. The samples were placed in a light-tight box and irradiated with a pulsed Q-switched Nd:YAG laser with the wavelength of 1064 nm, pulse width of 10 ns, pulse duration of 1 Hz and pulse enegy of 10 mJ.

3. Result and discussion

3.1 Crystal growth.

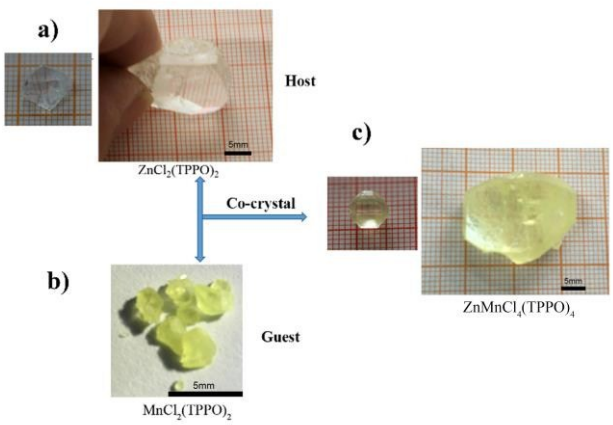

Fig. 2 Crystals of $ZnCl_2(TPPO)_2$ (a), $MnCl_2(TPPO)_2$ (b) and $MnZnCl_4(TPPO)_4$ (c).

The formation of co-crystalization depends on solubility[33], and the growth of separate crystals or co-crystalization depends on the beginning temperature and the rate at which the temperature is lowered. When these were not correct, only powder appeared in the bottom of the bottle during the lowering of the temperature. After several attempts, the starting temperature for $ZnMnCl_4(TPPO)_4$ crystal was chosen to be 55 ^oC. When the solution was cooled slowly to the room temperature at the speed of 0.5 ^oC /day, a bulk high quality light yellow crystal appeared at the bottom of the bottle. The $ZnMnCl_4(TPPO)_4$ crystals are approximately parallelepipeds and the crystals are like double-cones (see Fig. 2). During the process of crystal growth, specific strategies were applied to prevent the evaporation of ethanol. The appearance of the crystal was simulated by Materials Studio 4.4 software[34] and the exhibited facets were determined. (See Fig. S1 in ESI†)

At first, when high quality crystal of $ZnMnCl_4(TPPO)_4$ were removed from the solution at room temperature, the crystal cracked (see Fig. S2 and Fig.S3 in ESI†). To avoid this, after bulk crystal was grown, it was left in the bottle just above the solution for 1 day before it was taken out. Microcrystals appeared on the surface of the crystal (see Fig. 2) during the process of thermal equilibrium. After polishing, it exhibited the characteris- tics of a high quality single crystal.

3.2 Crystal structure.

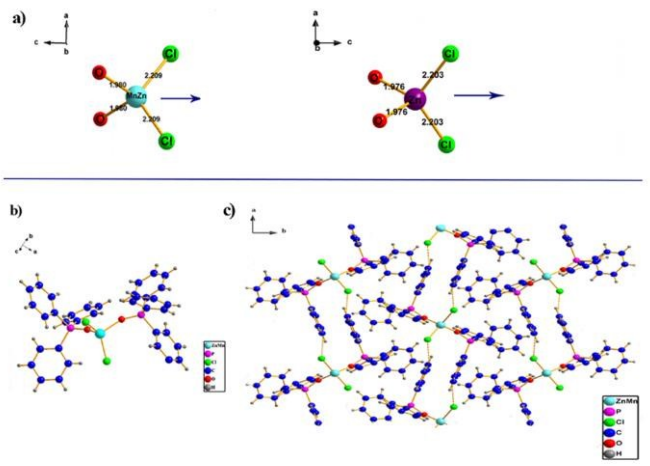

Fig. 3 (a) Ball-and stick diagram of the O_2•••Zn–Cl_2, O_2•••Mn–Cl_2 and O_2•••Zn–Cl_2 tetrahedral in a unit cell. Each tetrahedron is distorted, which gives rise to a net dipole moment antiparallel to the c direction (indicated by arrows). (b) Ball-and stick diagram of the $ZnMnCl_4(TPPO)_4$ crystal structure. (c) Part of the ball-and-stick diagram of the $ZnMnCl_4(TPPO)_4$ crystal along the c axis in a unit cell. The longer Zn–Cl or Mn–Cl bonds are always located in the upper direction in each O_2•••Zn–Cl_2 and O_2••• Mn–Cl_2 tetrahedron, giving rise to a net dipole moment antiparallel to the c axis.

Single-crystal X-ray diffraction data for and $ZnCl_2(TPPO)_2$ is presented in Table 1 and Table S1 in ESI†, respectively. The XRF data for $ZnMnCl_4(TPPO)_4$ is listed in Table S2 in ESI†. Crystallographic analysis reveals that both $ZnCl_2(TPPO)_2$ and $ZnMnCl_4(TPPO)_4$ belong to the orthorhombic systems with *F*dd2 (No.43) space group. For $ZnCl_2(TPPO)_2$, the cell parameters are a = 20.718 Å, b = 33.018 Å, c = 9.751 Å, V=6670(4) $Å^3$ and α=β=γ=90°; Z=4. This result is the same as reports of Rose[35]and Kosky[36]. For $ZnMnCl_4(TPPO)_4$, cell parameters are a = 20.7414 Å, b = 32.981 Å, c = 9.7539 Å, V=6672.4 (8) $Å^3$ and α=β=γ=90°, Z=8. Probably alternate zinc atoms, in the tetrahedral O_2•••Zn-Cl_2 and O_2•••Mn-Cl_2 structure unit is partly replaced by manganese atoms so that the distribution of zinc and manganese is random in the metal position. In crystallography test the electron diffraction distinction of Mn^{2+} and Zn^{2+} ions is tiny. In order to acquire accurate result, XRF analysis test was performed. The total proportion of Mn and Zn in the hybrid semi-organic crystal which is approximately equal to 1: 1 (0.46:0.54) is adopted finally and the crystal data was refined than.

A ball-stick diagram of the $ZnMnCl_4(TPPO)_4$ co-crystal structure is exhibited in Fig.3 and the structure of $ZnCl_2(TPPO)_2$ is similar. As shown in Fig. 3 and Table 2, the O_2•••Zn–Cl_2 and O_2•••Mn–Cl_2 structural unit is tetrahedral, and the macro-statistics average angle of O-Zn-O or O-Mn-O is 96.72(8)°; of O-Zn-Cl or O-Mn-Cl is 108.95(4)° and 112.18(4)°; and of Cl-Zn-Cl or Cl- Mn-Cl is 116.21(3)°. The macro-statistics average bond distance of Zn (1)-O or (Mn) (1)-O is 1.9796(12) Å; and of Zn(1)-Cl or Mn(1)-Cl, 2.2091(5) Å. As a result the O_2•••Zn–Cl_2 and O_2•••Mn–Cl_2 tetrahedral structure unit is distorted. In the $ZnMnCl_4(TPPO)_4$ crystal structure, the noncentrosymmetric O_2•••Zn–Cl_2 and O_2•••Mn–Cl_2 tetrahedral structure unit is irregularly arranged and gives rise to a three-dimensional asymmetric framework. The arrangement of the distorted tetrahedral structure results in the asymmetric structure of $ZnMnCl_4(TPPO)_4$ that exhibits SHG response.

3.2 Thermo Gravimetric Analysis and Differential Thermal Analysis.

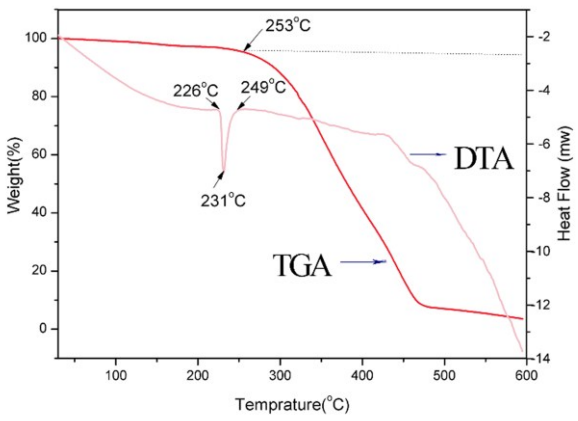

Fig.4 Thermo gravimetric and differential scanning calorimetry curves of the $ZnMnCl_4(TPPO)_4$ crystal.

The thermal behaviour of $ZnMnCl_4(TPPO)_4$ was obtained with thermo-gravimetric analysis and differential thermal analysis. With increasing temperature, the compound started to melt at 226 ^oC, a sharp endothermic peak appeared at 231^oC, and the

entire sample had melted by 249 °C. The sample was thermally stable up to 250 °C. However, between 250 °C and 450°C; the compound lost about 79% of its weight. This indicates that the residue is mainly TPPO (whose weight fraction in $ZnMnCl_4(TPPO)_4$ is 79%).

3.3 Optical properties.

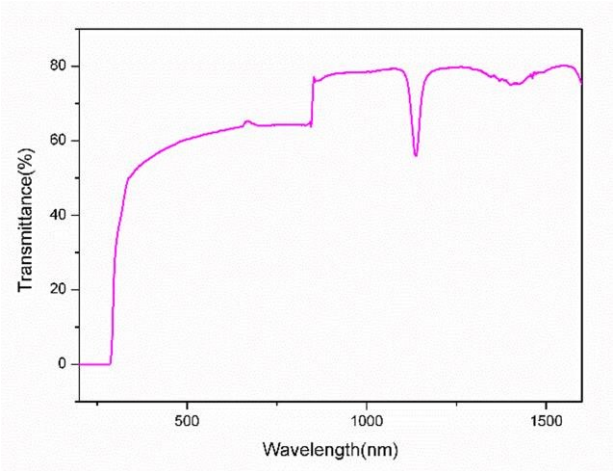

Fig.5 The transmittance spectrums of the $ZnMnCl_4(TPPO)_4$ crystal.

The transmittance spectrum and the UV–Vis diffuse reflectance spectra of the $ZnMnCl_4(TPPO)_4$ crystalline sample is shown in Fig.5 and Fig.6. The transmittance spectrum reveals that $ZnMnCl_4(TPPO)_4$ has a large transmission window from 500-1600nm and a high transmittance ratio (up to 80%). The UV-vis diffuse reflectance spectrum for $ZnMnCl_4(TPPO)_4$ is shown in Fig. 5. After the crystal was ground, it became colourless. The absorption spectrum of $ZnMnCl_4(TPPO)_4$ shows an absorption edge in the near UV at about 292 nm, indicating that the optical band gap of the crystal is approximately 4.25 eV, which is smaller than that of $ZnCl_2(TPPO)_2$ (4.3eV, see Fig S4 in in ESI†).

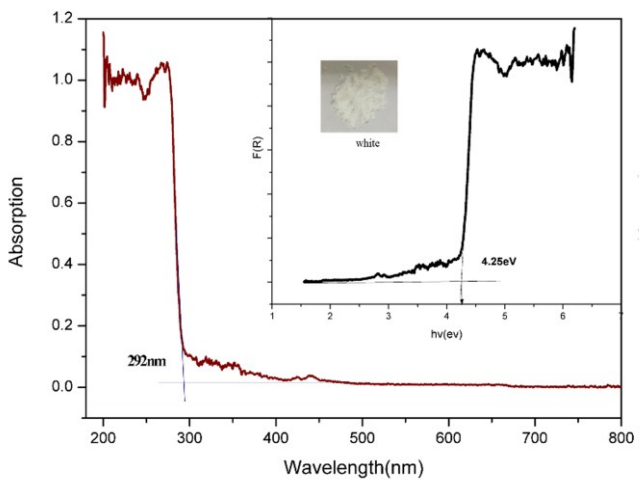

Fig. 6 UV-vis spectrum of ground powder of $ZnMnCl_4(TPPO)_4$ microcrystals.

The UV-vis absorption and fluorescence spectra together with a fluorescence image of a $ZnMnCl_4(TPPO)_4$ crystal are exhibited in Fig.7. Bright green light was observed with UV illumination at 365nm, and the fluorescence spectrum was excited by illumination at 390nm.

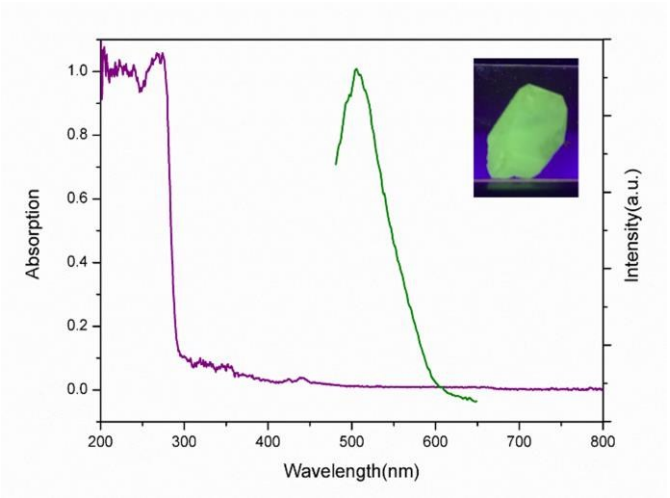

Fig. 7 UV-vis absorption and fluorescence spectra（excited at 390nm） and fluorescence image of $ZnMnCl_4(TPPO)_4$ crystal (excited at 365nm).

3.4 Hardness test.

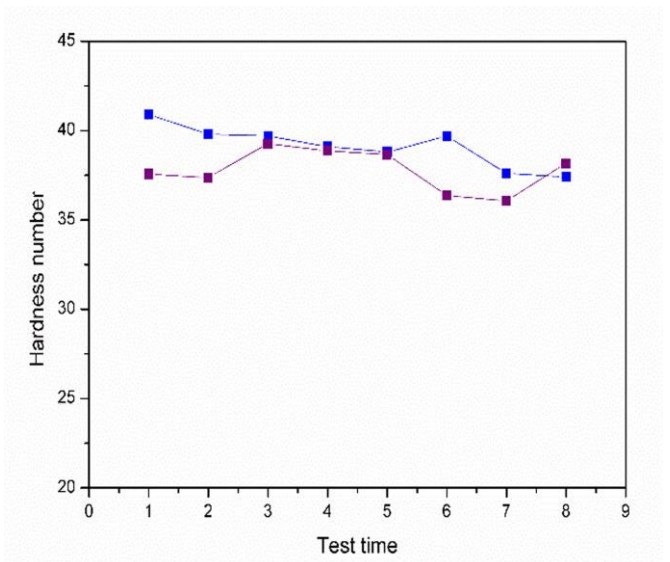

Fig.8 Hardness number of $ZnMnCl_4(TPPO)_4$ (blue) and $ZnCl_2$ $(TPPO)_2$ (purple) tested eight times.

The hardnesses of $ZnMnCl_4(TPPO)_4$ and $ZnCl_2(TPPO)_2$ are exhibited in Fig.7. After the test was performed eight times, the Hv_{min} and Hv_{max} were eliminated before averaging. The averages for $ZnMnCl_4(TPPO)_4$ and $ZnCl_2$ $(TPPO)_2$ are 39.1 and 37.8 respectively, indicating the Hm numbers are 2.29 and 2.27.

3.5 Magnetic property measurements.

The temperature dependence of the magnetic susceptibility of $ZnMnCl_4(TPPO)_4$ was measured in the temperature range of

5–300 K using a field of 1000 Oe. The χ_M^{-1}–T and χ_M–T plot in Fig. 8 proves that $ZnMnCl_4(TPPO)_4$ is paramagnetic. This confirms that the existence of a high proportion of Mn^{2+} in $ZnMnCl_4(TPPO)_4$ determines the magnetic properties. While in $Cu(TPPO)_4X_2 \bullet 2H_2O$ (X= Cl, Br) complex with one metal cation, four oxygen atoms and two chlorine atoms of the tetragonal bipyramide of $[CuO_4Cl_2]$ line in the equatorial and axial positions, respectively. The materials show ferromagnetic characteristic.[27]

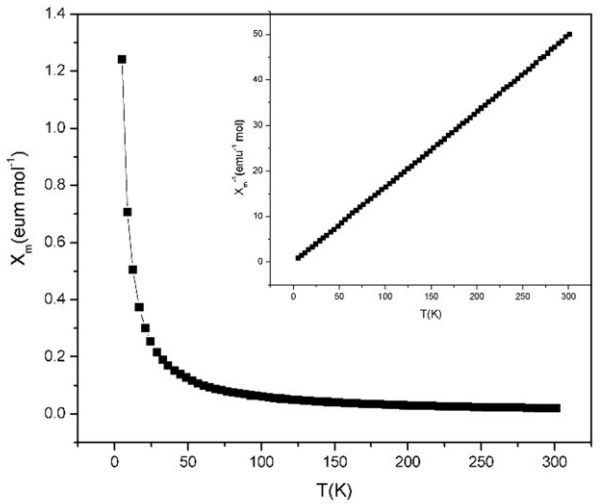

Fig.9 The temperature dependence of magnetic susceptibility of $ZnMnCl_4(TPPO)_4$ under a static field of 1000 Oe.

3.7 Second-harmonic generation measurements.

A Kurtz and Perry powder test was carried out to estimate the macroscopic nonlinearity of crystals of $ZnMnCl_4(TPPO)_4$ under the same performance conditions as KDP. The SHG in powder samples depends strongly on particle size as shown in Fig. 10. The intensity of the SHG signals initially increase gradually with the increase in particle size and then saturates for larger particle size. These are typical curves for phase-matchable materials.[32] These results reveal that the SHG response of $ZnMnCl_4(TPPO)_4$ is about twice that of KDP at 1064 nm, which is larger than that of $CdI_2(TPPO)_2$ with one metal cation.[28]

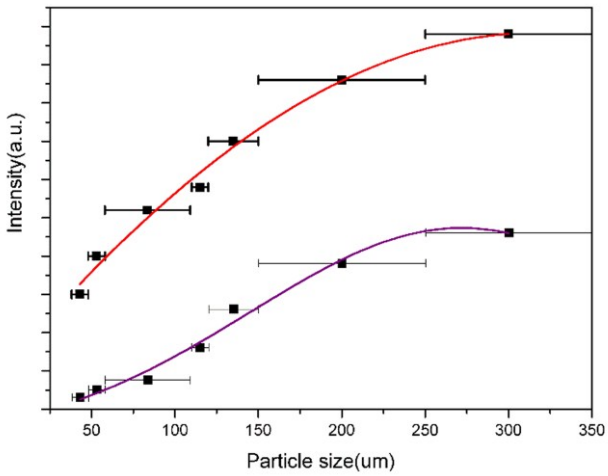

Fig. 10 Phase-matching curves for $ZnMnCl_4(TPPO)_4$ (red) and KDP (purple).

Conclusions

Bulk hybrid semi-organic crystals of $ZnMnCl_4(TPPO)_4$ have been successfully synthesized and grown using the temperature-lowering method through a design of guest-host combination for the first time. The powder SHG effect of $ZnMnCl_4(TPPO)_4$ is about twice that of KDP, which is larger than that of $CdI_2(TPPO)_2$ with one metal cation and phase-matching can be achieved. The material has relatively good thermal stability, a large band gap and excellent stability in air. In addition, it shows good magnetism and luminosity. Because of the variation of the coordination environment, $ZnMnCl_4(TPPO)_4$ exhibits paramagnetic character. Such kind of hybrid semi-organic crystals are potential multifunctional materials and detailed studies on the nonlinear optical properties of the crystals are under way.

Acknowledgements

The authors appreciate the help of Dr. Kenneth A. Jackson (member of National Academy of Engineering) and Professor Shengqing Xia, Wentao Yu for revising the manuscript and structure refinement, respectively. We thank the National Natural Science Foundation of China (Grant nos. 51321091, 51227002, 51272129) and the Program of Introducing Talents of Disciplines to Universities in China (111program no. b06015).

Notes and references

State Key Laboratory of Crystal Materials, Shandong University, Jinan, 250100, China.

Email: txt@sdu.edu.cn; ry@sdu.edu.cn.

†Electronic Supplementary Information (ESI) available: [CCDC 1442330 and 1057044, crystal morphology, photograph of $MnZnCl_4(TPPO)_4$, UV-

vis spectrum, crystal structure, XRF- SQX calculation]. See DOI: 10.1039/b000000x/

1 C. T. Chen, G. Z. Liu, *Annu. Rev. Mater. Sci.*, 1986, **16**, 203.
2 D. M. Burland, R. D. Miller and C. A. Walsh, *Chem. Rev.*, 1994, **94**, 31.
3 K. M. Ok, P. S. Halasyamani, *Chem. Soc. Rev.*, 2006, **35**,710.
4 Y.Y. Dang, X. G. Meng, K. Jiang, C. Zhong, X. G. Chen and J. G. Qin, *Dalton Trans*., 2013, **42**, 9893.
5 W. L. Smith, *Appl. Opt.*, 1977, **16**, 798.
6 F. C. Zumsteg, J. D. Birlein and T. E. Gier, *J. Appl. Phys.*, 1976, **47**, 4980.
7 C. T. Chen, Y. Wu, A. Jiang, B. Wu, G.You, R. Li and S. J. Lin, Opt. Soc. Am. B, 1989, **6**, 616.
8 C. T. Chen, B. Wu, A. Jiang and G. You, *Sci. Sin., Ser. B*, 1985, **28**, 235.
9 G. D. Boyd, R. C. Miller, K. Nassau, W. L. Band and A. Savage, *Appl. Phys. Lett.*, 1964, **5**, 234.
10 C. T. Chen, Y. Wang, Y. N. Xia, B. C. Wu, D. Y. Tang, K. C.Wu, W. R. Zeng, L. H.Yu, L. F. Mei, *J. Appl. Phys.*, 1995, **77**, 2268.
11 F. Pan, M. S. Wong, C. Bosshard, P. Günter, *Adv. Mater.*, 1996, **8**, 592.
12 W. G. Zhang, X. T. Tao, C. Q. Zhang, H. J. Zhang, M. H. Jiang, *Cryst. Growth Des.*, 2009, **9**,2633.
13 J. J. Zhang, X. T. Tao, Y. X. Sun, Z. H. Zhang, C. Q. Zhang, Z. L. Gao, H. B. Xia and S. Q. Xia, *Cryst. Growth Des.*, 2011, **11**, 1863.
14 W. G. Zhang, F. Li, S. H. Kim, P. S. Halasyamani, *Cryst. Growth Des.*, 2010, **10**, 4091.
15 P. Zhao, H. J. Cong, X. X. Tian, Y. X. Sun, C.Q. Zhang, S. Q. Xia, Z. L. Gao and Tao, X. T. *Cryst. Growth Des.*, 2015, **15**, 4484.
16 T. D. Kim, J. W. Kang, J. Luo, S. H. Jang, J. W. Ka, *J. Am. Chem. Soc*., 2007,**129**,488.
17 B. J. Coe, J. A. Harris, I. Asselberghs, K. Clays, G. Olbrechts, A. Persoons, *Adv. Funct. Mater.*,2002, **12**, 110.
18 S. R. Marder, J. W. Perry, W. P. Schaefer, *Science*, 1989, **245**, 626.
19 D. F. Eaton, A. G. Anderson, W. Tamm, Y.Wang, *In Polymers for High Technology Electronics and Photonics*; Ed. M. J. Bowden, R. S. Turner, American Chemical Society: Washington, D .C., 1987.
20 S. Tomaru, S. Zembutu, M. Kawachi, M. Kobayashi, *J. Inclusion Phenom*., 1984, **2**, 885.
21 H. Tabei, T. Kurihara, T. Kaino, *Appl. Phys. Lett*., 1987, **50**,1855.
22 I. W. Buch, M. L. Hav and L. L. Serowitz, *Chemistry of Materials*, 1989, **1**, 114.
23 N. Zhang, D. Yuan, X.T. Tao, D. Xu, Z. Shao, M. H. Jiang, M. Liu, *Opt. Commun.*, 1993, **99**, 247.
24 D. Xu, X. Q. Wang, W. T. Yu, S. X. Xu, G. H. Zhang, *J. Cryst. Growth*, 2003, **253**, 481.
25 X. Liu, X. Wang, X. Yin, S. Liu, W. He, L. Zhu, G. Zhang, D. Xu, *CrystEngComm*, 2014, **16**, 930.
26 G. F. Liu, J. Liu, X. X. Zheng, Y. Liu, D. S. Yuan, X. X. Zhang, Z. L. Gao and X. T. Tao, *CrystEngComm*, 2015, **17**, 2569.
27 D. Makanova, G. Ondrejovic, M. Melnik and J. Gazo, *Chem. Zvesti*, 1976, **30**, 73.
28 R. Santhakumari, K. Ramamurthi, H. Stoecklievans, R. Hemad, and W. Nirmala, *Physica B*, 2011, **406**, 1872.
29 Bruker *APEX2*, Bruker Analytical X-ray Instruments, Inc., Madison, Wisconsin, USA, 2005.
30 G. M.Sheldrick, *SHELXTL-97, Bruker Analytical X-ray Instruments*, Inc, Madison, WI, USA, 2003.
31 W. M.Wendlandt and H. G.Hecht, *Reflectance and Spectroscopy*, Inter science, New York, 1966, 62.
32 S. K. Kurtz and T. T. Perry, *J. Appl. Phys*., 1968, **39**, 3798.
33 A. Y. Li, L. L. Xu, J. M. Chen and T. B. Lu, *Cryst. Growth Des*., 2015, **15**, 3785.
34 Accelrys, *MS Modeling Getting Started*, Accelrys Software Inc., San Diego., 2006.
35 J. P. Rose, R. A. Lalancette, J. A. Potenza, H. J. Schugar, *Acta Crystallogr. B*, 1980, **36**, 2409.
36 C. A. Kosky, J. P. Gayda, J. F. Gibson, S. F. Jones, D. J. Williams, *Inorg. Chem*., 1982, **21**, 3173.